doi.org/10.15392/2319-0612.2026.3022
Braz. J. Radiat. Sci., Rio de Janeiro
2026, 14(2) | 01-22 | e3022
Editor(s): Dr. (Prof.) Bernardo Maranhão Dantas
Dr. (Prof.) Alfredo L. Ferreira Filho
Submitted: 2025-11-07
Accepted: 2026-02-19

Original Article

The Standardization of Cone Beam Computed Tomography (CBCT) Presets on the Elekta XVI System for Optimized Image-Guided Radiotherapy (IGRT)

Ribeiro [a*], V. A. B.; Yoriyaz [b], H.

[a] Instituto do Câncer do Estado de São Paulo, Hospital das Clinicas da Faculdade de Medicina da Universidade de São Paulo, São Paulo, São Paulo, Brazil.
[b] Instituto de Pesquisas Energéticas e Nucleares, São Paulo, São Paulo, Brazil.

*Correspondence: victor.bertotti@hc.fm.usp.br

Abstract: Image-Guided Radiotherapy (IGRT) relies on accurate imaging systems to ensure precise patient positioning and target localization. Cone-Beam Computed Tomography (CBCT) integrated into the Elekta XVI platform enables volumetric imaging with soft-tissue visualization, but image quality and patient dose strongly depend on acquisition parameters, or "presets." This study presents a comprehensive methodology for standardizing CBCT presets on the Elekta XVI system to optimize image quality, geometric accuracy, and radiation dose according to the ALARA (As Low As Reasonably Achievable) principle. Eighteen acquisition configurations were systematically evaluated by varying tube potential, tube current, exposure time, filtration, collimation, gantry speed, and projection number. Radiation dose was measured using a calibrated ionization chamber, while image quality was assessed through Catphan 503 phantom analysis using the PyLinac software, quantifying uniformity, contrast-to-noise ratio (CNR), spatial resolution (MTF), and geometric accuracy. Results showed that tube potential (kV) was the dominant factor influencing image uniformity ($\varrho = 0.674$, $p = 0.0229$) and contrast ($\varrho = 0.676$, $p = 0.0225$), while dose scaled linearly with tube current and exposure time. Bow-tie filtration (F1) reduced central dose by approximately 25% and improved CNR. Geometric accuracy remained within ±1 mm for all protocols. Based on these quantitative relationships, standardized clinical presets were established for distinct anatomical sites (Head and Neck, Chest, Prostate and Pelvis), combining higher tube potential with reduced mAs to balance photon penetration, image contrast, acquisition time, and dose efficiency. The resulting protocols ensure reproducible image quality, and minimized patient exposure. This framework demonstrates that data-driven standardization of CBCT presets enhances both safety and precision in daily IGRT practice and provides a foundation for future adaptive radiotherapy integration.

Keywords: Cone-Beam Computed Tomography (CBCT), Elekta XVI, image quality optimization, dose reduction, IGRT standardization.

doi.org/10.15392/2319-0612.2026.3022
Braz. J. Radiat. Sci., Rio de Janeiro
2026, 14(2) | 01-22 | e3022
Editor(s): Dr. (Prof.) Bernardo Maranhão Dantas
Dr. (Prof.) Alfredo L. Ferreira Filho
Submitted: 2025-11-07
Accepted: 2026-02-19

Padronização dos *Presets* de Tomografia Computadorizada de Feixe Cônico (CBCT) no Sistema Elekta XVI para Otimização da Radioterapia Guiada por Imagem (IGRT)

Resumo: A Radioterapia Guiada por Imagem (IGRT) depende de sistemas de imagem precisos para garantir o posicionamento adequado do paciente e a localização exata do alvo tumoral. A Tomografia Computadorizada de Feixe Cônico (CBCT), integrada à plataforma Elekta XVI, possibilita a aquisição de imagens volumétricas com visualização de tecidos moles; no entanto, a qualidade da imagem e a dose ao paciente dependem fortemente dos parâmetros de aquisição ou "*presets*". Este estudo apresenta uma metodologia abrangente para a padronização dos *presets* de CBCT no sistema Elekta XVI, visando otimizar a qualidade da imagem, a precisão geométrica e a dose de radiação, de acordo com o princípio ALARA (*As Low As Reasonably Achievable*). Foram avaliadas sistematicamente dezoito configurações de aquisição, variando-se o potencial do tubo, a corrente, o tempo de exposição, a filtração, a colimação, a velocidade do *gantry* e o número de projeções. A dose de radiação foi medida com uma câmara de ionização calibrada, enquanto a qualidade da imagem foi analisada por meio do fantoma Catphan 503 utilizando o *software* PyLinac, quantificando uniformidade, razão contraste-ruído (CNR), resolução espacial (MTF) e precisão geométrica. Os resultados mostraram que o potencial do tubo (kV) foi o principal fator que influenciou a uniformidade da imagem ($\rho = 0.674$, $p = 0.0229$) e o contraste ($\rho = 0.676$, $p = 0.0225$), enquanto a dose variou linearmente com a corrente e o tempo de exposição. A filtração tipo bow-tie (F1) reduziu a dose central em aproximadamente 25% e melhorou a CNR. A precisão geométrica manteve-se dentro de ±1 mm para todos os protocolos. Com base nessas relações quantitativas, foram estabelecidos *presets* clínicos padronizados para diferentes sítios anatômicos (Cabeça e Pescoço, Tórax, Próstata e Pelve), combinando maior potencial de tubo com menor produto mAs, equilibrando penetração de fótons, contraste da imagem, tempo de aquisição e eficiência de dose. Este trabalho demonstra que a padronização quantitativa e baseada em dados dos *presets* de CBCT aprimora simultaneamente a segurança e a precisão na prática clínica diária de IGRT, além de oferecer uma base sólida para futura integração em fluxos de radioterapia adaptativa.

Palavras-chave: Tomografia Computadorizada de Feixe Cônico (CBCT), Elekta XVI, otimização da qualidade de imagem, redução de dose, padronização em IGRT.

1. INTRODUCTION

Radiotherapy has increasingly relied on Image-Guided Radiotherapy (IGRT) to deliver high radiation doses precisely to the target volume while sparing surrounding healthy tissues. Among various IGRT techniques, Cone-Beam Computed Tomography (CBCT) has become the standard three-dimensional imaging modality due to its ability to provide volumetric images with good soft tissue contrast, which is crucial for accurate tumor localization.

However, the clinical effectiveness of CBCT is intrinsically linked to the configuration of the acquisition system. The CBCT source, a kilovoltage (kV) X-ray tube, allows adjustment of imaging parameters that directly impact both image quality and the radiation dose delivered to the patient. Since these imaging procedures contribute additional radiation exposure, understanding and managing this dose is critical to minimizing risks to sensitive organs and reducing the likelihood of secondary malignancies.

The AAPM Task Group 180 report provides a comprehensive overview of imaging doses associated with various modalities – including Megavoltage Electronic Portal Imaging (MV EPI), Kilovoltage Digital Radiography (kV DR), Tomotherapy MV-CT, MV Cone-Beam CT (MV-CBCT), and kV Cone-Beam CT (kV-CBCT) – and offers guidelines for dose calculation and patient dose management. TG 180 emphasizes the ALARA (As Low As Reasonably Achievable) principle in managing imaging dose and recommends that imaging dose should be accounted for in treatment planning if the cumulative dose from repeated imaging exceeds 5% of the prescribed therapeutic dose. This threshold reflects considerations of clinical relevance, organ dose tolerance, and practical feasibility in clinical workflows [1].

Imaging dose magnitude varies substantially depending on imaging frequency and technique. A single kV-CBCT acquisition typically delivers 1–9 cGy to soft tissues and 6–29 cGy to bone, the latter receiving a higher dose due to the dominance of the photoelectric effect in kV imaging. Cumulatively, repeated pelvic kV-CBCT scans can contribute an

additional 1%–3% of the prescription dose over the course of treatment. Thus, optimization strategies – such as reducing the imaging field size (e.g., cranial-caudal extent), tailoring imaging parameters (kVp, mAs) to anatomical sites, using partial rotation scan protocols to avoid critical superficial organs, and employing bow-tie filters – are crucial for minimizing dose while maintaining image quality. Clear communication of imaging dose among medical physicists and radiation oncologists is essential to enable informed clinical decisions, and the development of local imaging protocols is highly recommended [1].

Image quality in CBCT as it directly impacts, governing patient safety, geometric accuracy, and treatment success. Although CT-based IGRT systems demonstrate geometric accuracy within 1 mm, suitable for stereotactic body radiotherapy (SBRT) and conventional treatments, CBCT images are generally of lower quality compared to diagnostic CT due to cone-beam geometry and slower acquisition speeds. Common issues include increased noise and reduced contrast from scattered radiation, as well as inaccuracies in CT number (HU) values caused by scatter and beam hardening. These artifacts are especially critical when CBCT images are used for dose calculation in advanced adaptive radiotherapy programs [2].

Therefore, robust quality assurance (QA) programs are essential to maintain system performance and mitigate risks related to poor image quality. However, variability in CBCT acquisition parameters – such as kVp, mAs, filters, collimators, gantry rotation, and number of frames – complicates the selection of optimal settings for managing image quality and patient dose. The lack of standardized protocols limits clinical consistency and dose management.

Standardization of CBCT acquisition parameters is thus imperative. It enables clinics to manage the trade-off between image quality and imaging dose effectively, adhering to the ALARA principle. By commissioning and validating dose for each protocol, facilities can develop site-specific acquisition presets that minimize dose while preserving necessary image quality for distinct clinical tasks (e.g., visualization of bony anatomy versus soft tissues). This approach also promotes the consistent use of dose reduction techniques,

including bow-tie filters and partial rotations, which have demonstrated significant dose savings—especially important for smaller anatomical sites. Moreover, standardized protocols streamline clinical workflow, facilitate operator use, ensure documentation of QA findings, and support patient safety.

The objective of this work was to standardize the CBCT acquisition parameters (presets) for the XVI system. This standardization aimed to reduce user variability and ensure the high accuracy necessary for clinical application in radiotherapy patients. The process involved a comprehensive evaluation of the dose versus image quality trade-off across various technical parameters.

2. MATERIALS AND METHODS

The study was conducted using an Elekta Axesse linear accelerator (Elekta, Stockholm, Sweden) equipped with the XVI® imaging system (version 5.0.7.1), located at the Instituto do Câncer do Estado de São Paulo (ICESP).

The XVI system utilizes a kilovoltage (kV) X-ray source in combination with an amorphous silicon flat-panel detector. The following acquisition parameters were investigated: tube potential (70, 100, and 120 kV), tube current (10, 32, and 64 mA), exposure time (10, 20, and 40 ms), collimator size (S20, M20, and L20), filtration (F0, neutral; F1, bow-tie filter), gantry rotation speed (180°/min or 360°/min), and number of frames (330 or 660). A total of 18 acquisition configurations (labeled A–R) were evaluated to assess the influence of each parameter on radiation dose and image quality.

2.1. Dose Measurement Methodology

Absolute dose measurements were performed to establish reference values and to assess the influence of beam and geometric parameter variations. A Farmer-type ionization chamber (PTW TN 30013, S/N 04515) was previously cross-calibrated against a reference

chamber (Radcal Corporation® 10×6-0.6CT) using cylindrical acrylic phantoms. Measurements were conducted for four beam qualities (Q1–Q4) at 100 kV and 120 kV, with F0 and F1 filtrations, and S20, M20, and L20 collimators. The mean calibration factor determined from these measurements was 4.9003 ± 0.0364 cGy/nC [3].

Subsequent absolute dose measurements were carried out with the calibrated Farmer chamber positioned at the center (7.5 cm depth) of the solid water phantom (30 × 30 × 15 cc).

2.2. Image Quality Measurement Methodology

Image quality evaluations were performed using the Catphan 503 phantom. Data analysis was conducted with the PyLinac library (version 3.28.0).

Uniformity was assessed using the CTP486 module (Figure 1). This metric quantifies the consistency of Hounsfield Units (HU) across a uniform region of the phantom. The Image Uniformity Index (UI – Equation 1) compares the mean HU values in the peripheral regions to those in the central region of the Catphan. Ideally, UI values approach zero, with larger deviations indicating reduced uniformity. Similarly, the Integral of Non-uniformity (IN – Equation 2) can also estimate uniformity; both UI and IN are automatically calculate by the PyLinac software [4].

$$UI = 100\,.\frac{\overline{HU}_{periphery} - \overline{HU}_{center}}{\overline{HU}_{center} + 1000} \quad (1)$$

$$IN = \frac{\overline{HU}_{max} - \overline{HU}_{min}}{\overline{HU}_{max} + \overline{HU}_{min} + 2000} \quad (2)$$

Spatial resolution was objectively evaluated using the Modulation Transfer Function (MTF) derived from the CTP528 module (Figure 1). High-contrast spatial resolution refers to the scanner's ability to distinguish small, high-contrast objects. It can be assessed visually – via line pair patterns (lp/cm) – or quantitatively using the MTF, which is calculated from the point spread function (PSF) of a wire or line. The MTF describes the system's response as a function of different spatial frequencies; higher resolutions correspond to greater MTF

values at higher frequencies. The CTP528 module contains 21 sets of aluminum wire pairs of varying thicknesses, whose peaks and troughs are used to compute and normalize the MTF with respect to the first line pair [5].

Geometric accuracy was verified by measuring the distances between known features, specifically, air and Teflon rods spaced at 5 cm intervals in the CTP404 module (Figure 1).

Figure 1: Catphan CTP486 module (a.), CTP528 module (b.), and CTP404 module (c.).

a. b. c.

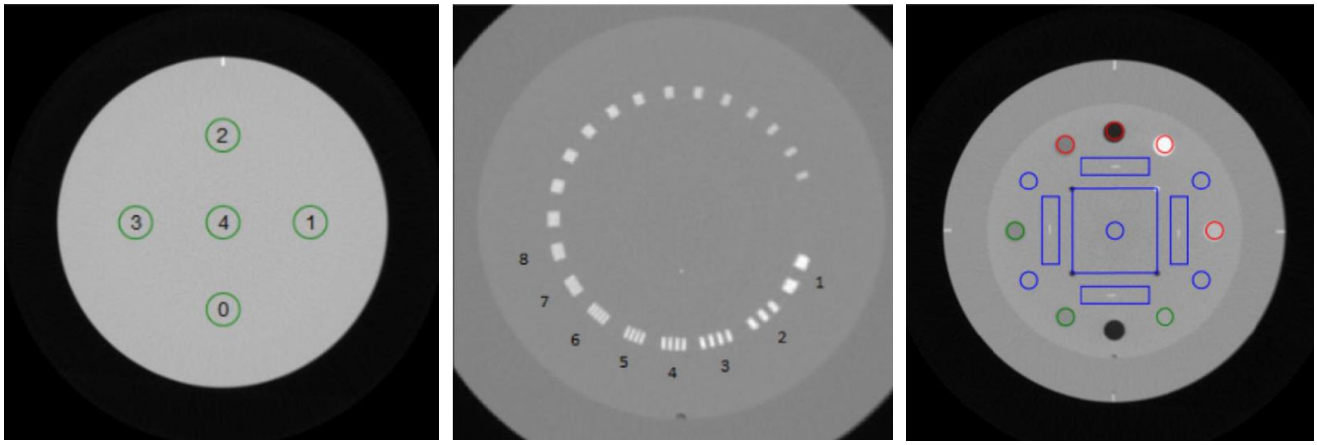

The Contrast-to-Noise Ratio (CNR) quantifies the system's ability to distinguish structures with different densities in the presence of image noise. In medical physics, the Catphan phantom is widely used for this purpose, enabling an objective and reproducible evaluation of scanner performance. The CNR is calculated according to Equation 3, which considers the mean Hounsfield Unit difference between low-contrast materials (such as LDPE and Polystyrene) and the associated noise in each region. Higher CNR values indicate improved system performance in representing subtle contrast differences, which is critical for the detection of low-contrast lesions and for optimizing imaging protocols while maintaining minimal patient dose.

$$CNR = 2 * \frac{\overline{HU}_{LDPE} - \overline{HU}_{Poly}}{Noise_{LDPE} + Noise_{Poly}} \quad 3$$

As well as the uniformity indices, MTF at 50% intensity, CNR, and geometric accuracy were automatically calculated by PyLinac software.

3. RESULTS AND DISCUSSIONS

A total of 18 Cone-Beam Computed Tomography (CBCT) acquisition configurations (Table 1) were systematically evaluated to characterize how beam parameters affect radiation dose, image quality, and geometric accuracy in the Elekta XVI system. The results reveal consistent physical trends and clinically relevant relationships between dose, contrast, uniformity, and acquisition settings, allowing for the establishment of optimized and standardized presets for Image-Guided Radiotherapy (IGRT).

3.1. Dose Behavior and Physical Dependencies

The magnitude of the measured doses strongly depends on the phantom geometry and does not fully represent the actual doses received by patients undergoing IGRT. In addition, variations in the composition of different anatomical structures lead to differences in energy deposition, particularly in bone tissues, which exhibit an enhanced photoelectric effect [6]. Nevertheless, the doses measured in this study are intended for relative analysis, providing a consistent basis for assessing dose reduction to the patient.

Radiation dose increased consistently with beam energy and exposure parameters. The dependence on tube potential (kV) followed a second-order polynomial trend, while tube current (mA) and exposure time (ms) exhibited a nearly perfect linear correlation with dose ($R^2 = 1$) – Figure 2. These findings are consistent with the fundamental proportionality between tube output and the product of current and time (mAs), as previously demonstrated by Al-Kabkabi et al. (2022), who reported a strong linear correlation ($R^2 = 0.899$) between imaging dose and mAs. The present data confirm that dose modulation in CBCT is primarily governed by total photon fluence rather than beam filtration or gantry motion, supporting the physical validity of dose prediction models proposed in prior optimization studies [7].

Figure 2: Measure dose in function of Tube Energy (a.), Tube Current (b.) and Exposition Time (c.).

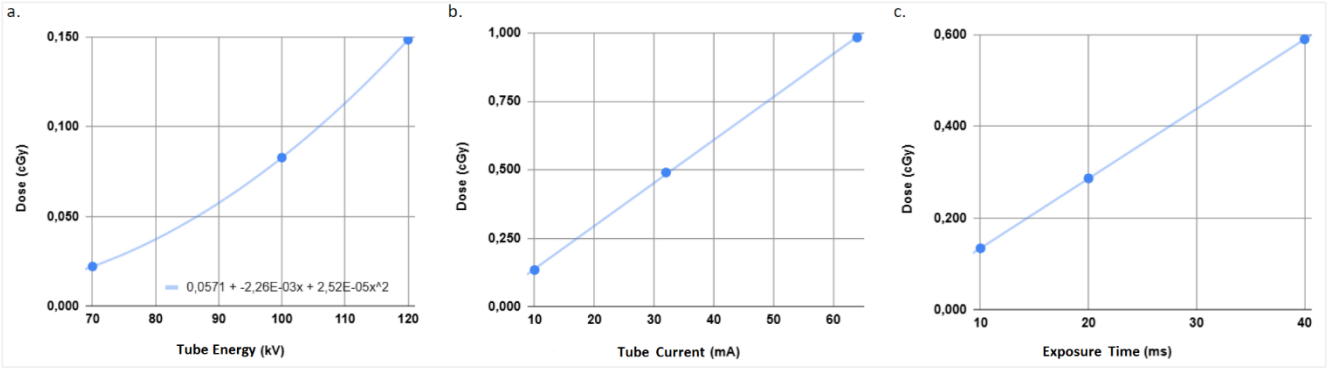

Table 1: Dose and image quality results for different CBCT acquisition parameters. ***Values in bold indicate the parameters being varied.***

CONFIGURATION	TUBE POTENTIAL (kV)	TUBE CURRENT (mA)	EXPOSURE TIME (ms)	COLLIMATOR SIZE	FILTRATION	GANTRY SPEED (°/min)	ROTATION DIRECTION	NUMBER OF PROJECTIONS	DOSE (cGy)	ACQUISITION TIME (MM:SS)	GEOMETRIC DISTANCE (mm)	MTF 50% (mm^{-1})	UNIFORMITY INDEX (UI)	INTEGRAL OF NON-UNIFORMITY (IN)	CNR
A	***70***	10	10	S20	F0	360	CW	183	0.020	-	50.01	0.23	13.16	0.062	0.4
B	***70***	10	10	S20	F0	360	CC	183	0.024	-	-	-	-	-	-
C	***100***	10	10	S20	F0	360	CW	183	0.075	-	50.00	0.24	4.42	0.022	0.9
D	***100***	10	10	S20	F0	360	CC	183	0.091	-	-	-	-	-	-
E	***120***	***10***	***10***	S20	F0	360	CW	183	0.134	01:19	49.95	0.24	1.29	0.010	1.8
F	***120***	10	10	S20	F0	360	CC	183	0.163	-	-	-	-	-	-
G	120	***32***	10	S20	F0	360	CW	183	0.490	-	49.95	0.24	2.09	0.012	3.1
H	120	***64***	10	S20	F0	360	CW	183	0.983	-	50.00	0.24	1.99	0.011	4.3
I	120	10	***20***	S20	F0	360	CW	183	0.287	-	49.97	0.24	1.31	0.012	2.4
J	120	10	***40***	S20	F0	360	CW	183	0.590	-	49.96	0.24	1.64	0.012	3.0
K	120	20	20	M20	***F0***	360	CW	660	1.064	-	49.84	0.23	2.38	0.012	3.7
L	120	20	20	M20	***F1***	***360***	CW	***660***	0.807	02:16	49.87	0.23	2.51	0.012	4.3
M	120	20	20	M20	F1	***180***	CW	660	1.035	02:51	49.90	0.23	2.64	0.013	3.9
N	120	20	20	M20	F1	360	CW	***330***	0.803	02:15	49.84	0.23	2.63	0.013	3.8
O	120	20	20	L20	***F0***	360	CW	660	0.804	-	-	-	-	-	-
P	120	20	20	L20	***F1***	***360***	CW	***660***	0.611	02:17	-	-	-	-	-
Q	120	20	20	L20	F1	***180***	CW	660	0.766	02:49	-	-	-	-	-
R	120	20	20	L20	F1	360	CW	***330***	0.609	02:17	-	-	-	-	-

Note: Image-quality metrics were not assessed for the L20 collimator (configuration O, P, Q and R), as it is not routinely used in our institution due to its broader irradiation field. It is reserved for specific cases requiring extended anatomical coverage or evaluation of superficial structures.

3.2. Contrast-to-Noise Ratio (CNR) and Image Noise

Image contrast showed a proportional increase with total exposure. Increasing tube current from 10 mA to 64 mA raised the CNR from 1.8 to 4.3, confirming that higher mAs reduces image noise and enhances low-contrast detectability. Similar trends were observed by Al-Kabkabi et al. (2022), who reported CNR increases from 1.7 to 2.3 for brain and body protocols, respectively, under analogous exposure escalations. The present results thus confirm that image quality in kV-CBCT is strongly exposure-limited, and improvements in CNR come at the expense of dose [7].

The relationship between CNR and dose demonstrated a strong positive correlation ($R^2 = 0.955$, $p < 0.001$), consistent with theoretical expectations from X-ray signal statistics and with empirical observations from Wilson et al. (2025). These authors also emphasized that optimization requires locating the "dose-efficiency plateau," where further dose increases no longer yield meaningful CNR gains – a trend mirrored in our data, in which CNR improvements saturated beyond 0.6–0.8 cGy (Figure 3) [8].

Figure 3: Dose–CNR trade-off curve showing the relationship between radiation dose and image quality.

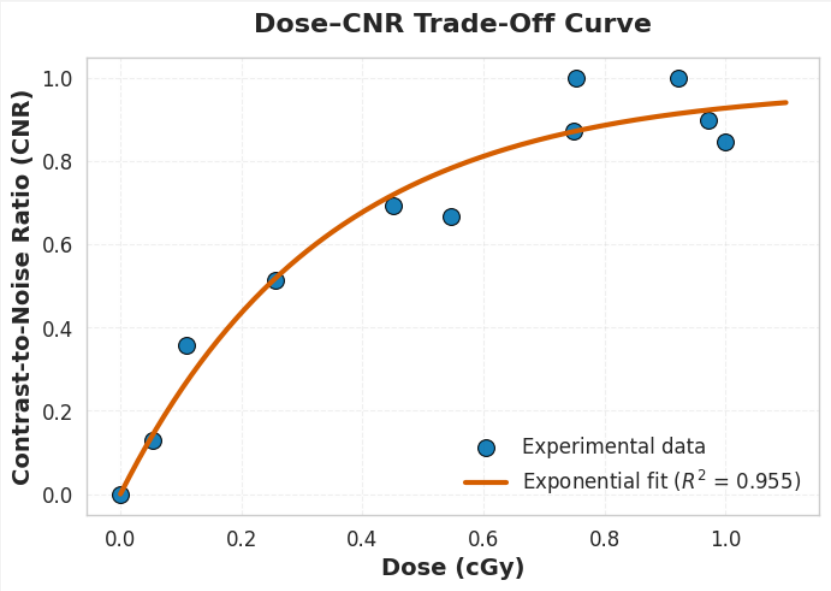

3.3. Influence of Filtration and Beam Energy

The introduction of the bow-tie filter (F1) resulted in a substantial improvement in imaging performance. Compared with the neutral filter (F0), F1 reduced central phantom dose by 24%, in agreement with Downes et al. (2009) and consistent with the 23.9% attenuation reported experimentally and 22.2% ± 1.8% from Monte Carlo simulations. In our measurements, this reduction in dose was accompanied by an increase in CNR from 3.7 to 4.3, corroborating the results of Al-Kabkabi et al. (2022), who found that bow-tie filtration enhances contrast by mitigating scatter. The F1 filter's dose-saving and contrast-enhancing properties thus establish it as a critical element of protocol optimization, however, due to its geometry, it is only used in protocols with full acquisition rotation (360 degrees) [6,7].

Furthermore, increasing tube potential from 70 to 120 kV improved both uniformity and CNR, with significant correlations between kV and UI ($\varrho = 0.674$, $p < 0.05$) and between kV and CNR ($\varrho = 0.676$, $p < 0.05$), Table 2. These effects stem from increased photon penetration and reduced beam hardening, leading to more homogeneous image intensities. The findings align with those of Wilson et al. (2025), who reported similar enhancements in uniformity and contrast with energy escalation, but also cautioned that dose increases exponentially with kV, emphasizing the need for controlled optimization [8].

3.4. Uniformity and Cupping Artifacts

Uniformity evaluation using the Catphan CTP486 module showed best results (UI = 1.29) for the lowest current and exposure time configuration (E). However, higher-dose protocols exhibited slight degradation in uniformity (UI = 2.0–2.6) due to cupping artifacts (central darkening caused by scattered radiation and nonuniform beam attenuation). These findings are consistent with Kamath et al., who demonstrated that large deviations of the UI from zero correspond to cupping intensity, particularly at high mAs levels where scatter correction algorithms reach their limits [9].

The Integral Non-Uniformity (IN) and UI metrics exhibited nonlinear dependencies on exposure parameters, although both metrics improved with increasing kV. As in Al-Kabkabi et al. (2022), the UI metric proved more sensitive than IN for quantifying uniformity variations, suggesting that UI may be preferred for detecting beam-hardening artifacts in QC routines [7].

3.5. Spatial Resolution and Geometric Accuracy

Spatial resolution, quantified by MTF 50%, remained nearly invariant (0.24 mm^{-1}) across all tested configurations, indicating that resolution is primarily determined by system geometry and reconstruction algorithms rather than exposure settings. This agrees with both Wilson et al. (2025) and Al-Kabkabi et al. (2022), who observed minimal impact of kVp and mAs variations on high-contrast resolution. Al-Kabkabi et al. reported MTF 50% values of 0.37–0.52 lp mm^{-1} across protocols, a little better than those comparable to measured in our study. In both investigations, the lowest mAs presets (Head/Neck) achieved the highest spatial resolution, whereas high-dose body protocols exhibited slightly lower MTF responses, reinforcing that resolution is hardware-dominated rather than dose-dependent [7,8].

Geometric accuracy, verified using the CTP404 module, was consistently maintained within ±1 mm across all acquisitions, meeting AAPM TG-179 tolerances and confirming the Elekta XVI system's mechanical stability for stereotactic and conventional IGRT applications [2].

3.6. Effect of Gantry Speed, Rotation Direction, and Number of Projections

Reducing gantry speed from 360°/min to 180°/min resulted in a 26.9% increase in total dose and acquisition time by 33 s while slightly decreasing CNR from 4.3 to 3.9. This inverse trend demonstrates that slower rotations extend exposure duration without improving image quality, consistent with the findings of Wilson et al. (2025), who reported a 100% dose increase

when halving gantry speed and doubling projections. Hence, maintaining 360°/min ensures optimal dose efficiency without compromising image metrics [8].

Similarly, halving the number of projections from 660 to 330 produced negligible changes in dose or time but reduced CNR by 12%. Al-Kabkabi et al. (2022) simulated this effect by reconstructing images from partial projection sets, showing that reducing projections by 75% halved the CNR and tripled the image noise (SD increase from 5.6 to 8.2 HU to low-density polyethylene – LDPE). Our experimental results confirm that sufficient projection sampling is essential for maintaining low noise and stable CNR performance [7].

Rotation direction had a minor but measurable influence: counterclockwise (CC) rotations delivered 21% more dose than clockwise (CW) acquisitions, likely due to mechanical asymmetries in tube rotation efficiency or calibration offsets. Although not statistically significant, this finding underscores the importance of verifying system-specific performance before protocol finalization.

3.7. Correlation Analysis and Optimization Implications

Given that several acquisition parameters (tube potential, filtration, gantry speed, and number of projections) are discrete or ordinal variables and may exhibit non-linear monotonic relationships with dose and image quality metrics, correlation analysis was performed using Spearman's rank correlation coefficient (ϱ). Spearman correlation does not assume linearity or normal distribution and is therefore more appropriate for evaluating monotonic dependencies in CBCT acquisition parameter optimization. Statistical significance was defined as $p < 0.05$. Spearman correlation analysis summarized these dependencies quantitatively – Table 2.

Table 2: Spearman correlation coefficients between the independent exposure parameters and the image quality/dose metrics. ***Values in bold indicate the parameters statistically significant*** **p** ***< 0.05.***

Independent Variable	DOSE (cGy)	p	UNIFORMITY INDEX (UI)	p	CNR	p
TUBE POTENTIAL (kV)	***0.674***	***0.0229***	***0.674***	***0.0229***	***0.676***	***0.0225***
TUBE CURRENT (mA)	***0.695***	***0.0177***	-0.039	0.9091	***0.816***	***0.0022***
EXPOSURE TIME (ms)	0.503	0.1152	0.141	0.6799	0.348	0.2950
FILTRATION – F1	0.452	0.1630	-0.387	0.2393	***0.615***	***0.0442***
GANTRY SPEED (°/min)	-0.400	0.2229	0.300	0.3701	-0.301	0.3689
NUMBER OF PROJECTIONS	***0.746***	***0.0084***	-0.341	0.3046	***0.630***	***0.0376***

Dose showed strong positive correlations with tube potential (ϱ = 0.674, p = 0.0229), tube current (ϱ = 0.695, p = 0.0177) and number of projections (ϱ = 0.746, p = 0.0084). Among image-quality parameters, the Uniformity Index correlated most strongly with tube potential (ϱ = 0.674, p = 0.0229); and the CNR correlated with both dose (ϱ = 0.87, p = 0.0005 – Figure 4), tube potential (ϱ = 0.676, p = 0.0225), tube current (ϱ = 0.816, p = 0.0022), filtration-F1 (ϱ = 0.615, p = 0.0442) and number of projections (ϱ = 0.630, p = 0.0376). These statistically significant relationships confirm that the tube potential is the driver of both uniformity and contrast, although contrast is dependent on other variables.

These findings are in close agreement with Wilson et al. (2025), who also identified tube potential as the dominant factor affecting uniformity and CNR in XVI systems, and with Al-Kabkabi et al. (2022), who reported similar correlation magnitudes across multi-institutional datasets. The consistency across independent studies reinforces the generalizability of these optimization trends for clinical standardization [7,8].

Figure 4: Spearman correlation matrix between CBCT acquisition parameters, image quality metrics, and radiation dose.

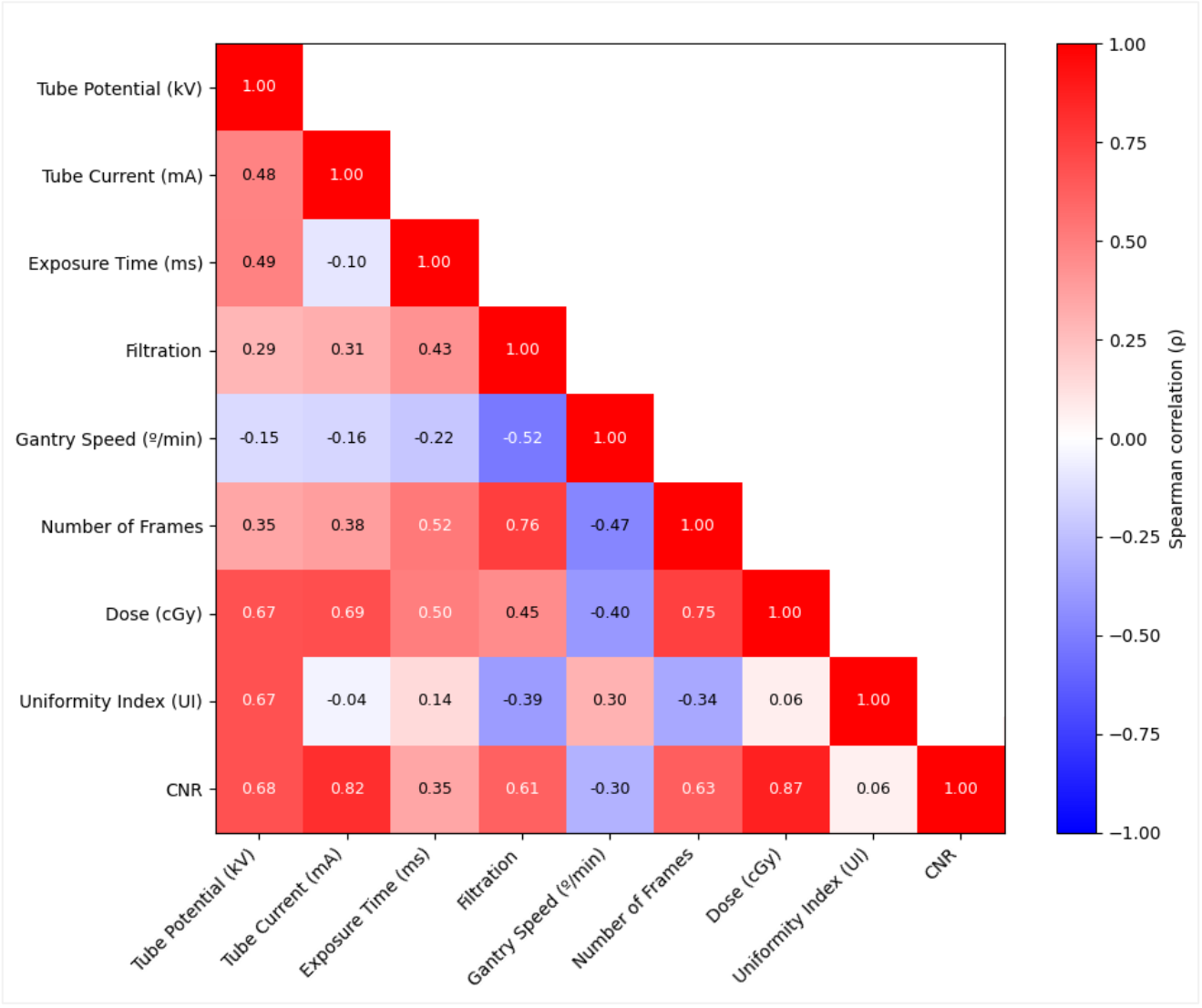

3.8. Clinical Standardization and Practical Recommendations

Based on these quantitative assessments, optimized presets were defined by anatomical site – Table 3. For small fields (S20 collimator), a 200° partial-arc rotation was standardized to reduce dose and acquisition time while maintaining adequate image quality for soft-tissue registration. For larger anatomical regions (M20, L20), full 360° rotations with F1 filtration were preserved to maximize CNR and uniformity. These standardized presets ensure geometric precision (-0.16 mm maximum deviation for K and N configuration) and

consistent image quality across clinical applications, matching or exceeding the performance benchmarks reported by Wilson et al. (2025) [8].

Considering the observed correlations and the physical behavior of dose and image quality, the final standardized presets prioritized protocols using higher tube potential (kV) combined with lower tube current–time product (mAs). This configuration was selected to enhance photon penetration and improve the Contrast-to-Noise Ratio (CNR) while minimizing the overall imaging dose. Increasing kV provides a more homogeneous beam and reduces image noise due to better tissue penetration, whereas lowering mAs effectively limits patient exposure. This balance follows the optimization strategy described by Wilson et al. (2025) and Al-Kabkabi et al. (2022), who demonstrated that maintaining adequate beam energy while reducing mAs achieves superior image quality–to-dose efficiency in CBCT systems, consistent with the ALARA principle [7,8].

The combined analysis highlights that CBCT optimization cannot rely on fixed "universal" settings but must be guided by systematic evaluation of dose-quality trade-offs. Both Wilson et al. and Al-Kabkabi et al. emphasize that the goal of standardization should be methodological rather than prescriptive: institutions should standardize how optimization is performed – through quantitative QA, dose tracking, and image-quality verification – rather than enforcing a single set of acquisition parameters. The present work adopts and extends this philosophy, providing an evidence-based framework for reproducible CBCT optimization [7,8].

Table 3: Standardized CBCT Acquisition Parameters (Presets).

Preset Name	Tube Energy (kV)	Tube Current (mA)	Exposure Time (ms)	Milliampere-seconds (mAs)	Collimator Size	Filtration	Gantry Speed (°/min)	Rotation Direction	Number of Projections
Fast Head and Neck S20 CW	120	10	10	65	S20	F0	360	CW	183
Fast Head and Neck S20 CC	120	10	10	65	S20	F0	360	CC	183
Fast Chest S20 CW left	120	16	16	166.4	S20	F0	360	CW	183
Fast Chest S20 CC right	120	16	16	166.4	S20	F0	360	CC	183
Fast Prostate S20 CW	120	16	16	166.4	S20	F0	360	CW	183
Fast Prostate S20 CC	120	16	16	166.4	S20	F0	360	CC	183
Chest M20 CW	120	20	20	260	M20	F1	360	CW	660
Chest M20 CC	120	20	20	260	M20	F1	360	CC	660
Pelvis M20 CW	120	32	20	416	M20	F1	360	CW	660
Pelvis M20 CC	120	32	20	416	M20	F1	360	CC	660
Pelvis L20 CW	120	64	40	1664	L20	F1	360	CW	660
Pelvis L20 CC	120	64	40	1664	L20	F1	360	CC	660

3.9. Summary and Clinical Implications

The standardized imaging configurations established in this work combine higher tube potential (kV) with reduced mAs to enhance photon penetration and improve the CNR while maintaining imaging doses as low as reasonably achievable. Increased beam energy reduces image noise and enhances tissue penetration, leading to more homogeneous projection data, whereas lowering mAs directly decreases patient exposure. This approach aligns with the optimization framework proposed by Wilson et al. (2025) and Al-Kabkabi et al. (2022), who demonstrated that maintaining elevated kV with moderate mAs yields optimal image quality-to-dose efficiency in kV-CBCT acquisitions [7,8].

Bow-tie filtration (F1) was therefore adopted as the standard for medium and large collimations (M20 and L20) due to its well-established benefits in attenuating peripheral scatter, improving image uniformity, and reducing central dose by approximately 25%. These effects were consistent with both our measurements (section 3.3) and the reductions reported by Al-Kabkabi et al. (2022) [7].

Furthermore, partial-arc acquisitions (~200°) were intentionally implemented for small-field presets to minimize unnecessary irradiation of superficial organs at risk (OARs) while preserving sufficient image quality for accurate target localization. For instance, in breast imaging, the chosen angular ranges were designed to avoid irradiation of contralateral tissues – Table 4 and Figure 5. This angular optimization is consistent with the findings of Wilson et al. (2025), who showed that asymmetric or partial arcs can substantially reduce skin and superficial organ doses without compromising image registration accuracy [8].

Overall, the standardization process emphasized a balanced and quantitative optimization strategy. Rather than maximizing a single image-quality metric, each protocol was designed to achieve a stable and clinically meaningful equilibrium among contrast, noise, geometric fidelity, and dose efficiency. The resulting standardized presets enable predictable image performance, reduced operator variability, improved patient safety, and enhanced reproducibility, supporting the requirements of high-precision and adaptive image-guided radiotherapy (IGRT).

Ultimately, effective optimization necessitates the development of protocols tailored to specific patient sizes and clinical applications. While reducing mAs can achieve dose reductions for a significant proportion of patients, specific applications, such as Stereotactic Radiosurgery (SRS), may require increasing mAs to enhance visual detection of soft tissue targets, resulting in a proportional increase in imaging dose. This flexibility supports optimization, allowing certain patients (e.g., those requiring superior image quality or those of larger size) to receive higher-than-default doses when clinically warranted. Al-Kabkabi et al. (2022) [7].

Table 4: Schematic representation of the irradiated angular sectors during partial-arc CBCT acquisition.

Protocol	Aquisition diretion	MV beam Initial-Final	kV beam Initial-Final
A	CC	20º-180º	110º-270º
B	CW	340º-180º	70º-270º
C	CW	70º-230º	160º-320º

Figure 5 : Representation of the irradiated angular area during partial-arc CBCT acquisition.

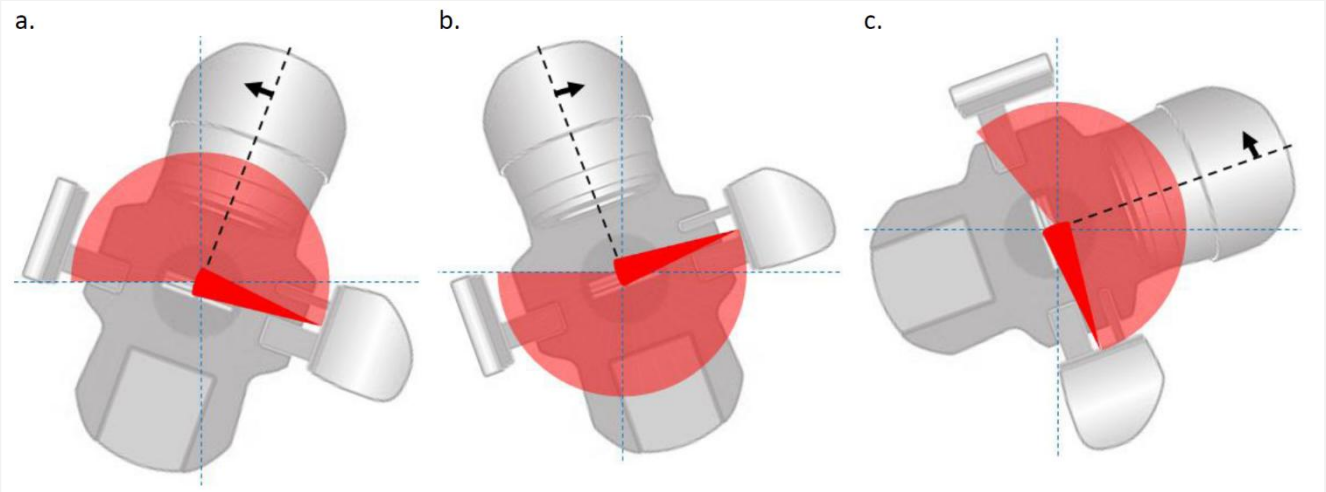

The standardized presets derived from this study offer a practical foundation for clinical implementation of CBCT-guided radiotherapy, ensuring reproducible image quality, reduced patient exposure, and alignment with international QA recommendations. The approach demonstrates that rigorous, data-driven standardization can harmonize safety and precision in daily IGRT practice while facilitating future integration of quantitative CBCT in adaptive workflows.

4. CONCLUSIONS

This study established a systematic framework for the standardization of Cone-Beam Computed Tomography (CBCT) acquisition presets on the Elekta XVI system, with the objective of optimizing image quality while minimizing patient dose in accordance with the ALARA principle. Through a comprehensive quantitative evaluation encompassing 18 acquisition configurations, the results demonstrated that tube potential (kV) is the dominant parameter influencing both image uniformity and contrast, while tube current and exposure time primarily govern total dose. Filtration and projection sampling showed secondary but relevant effects, providing additional flexibility for fine-tuning clinical protocols.

The standardized presets derived from this study offer a practical foundation for clinical implementation of CBCT-guided radiotherapy, ensuring reproducible image quality, reduced patient exposure, and alignment with international QA recommendations. The approach demonstrates that rigorous, data-driven standardization can harmonize safety and precision in daily IGRT practice while facilitating future integration of quantitative CBCT in adaptive workflows.

In conclusion, this study provides an evidence-based framework for the commissioning and standardization of CBCT acquisition parameters on the Elekta XVI system. The results validate the reproducibility of dose–quality relationships observed in prior literature, confirm the feasibility of achieving dose reductions without compromising geometric accuracy, and demonstrate that optimized preset standardization is both achievable and clinically advantageous. By combining systematic QA testing, statistical correlation analysis, and clinical feasibility assessment, this work establishes a robust foundation for safer, more efficient, and more consistent image-guided radiotherapy practices.

CONFLICT OF INTEREST

All authors declare that they have no conflicts of interest.

DATA AVAILABILITY STATEMENT

The authors declare that the data supporting the results of this study are available in the article. Derived data supporting the conclusions of this study are available upon request from the corresponding author.

REFERENCES

[1] DING, G. X.; ALAEI, P.; CURRAN, B.; FLYNN, R.; GOSSMAN, M.; MACKIE, T. R.; MIFTEN, M.; MORIN, R.; XU, X.; ZHU, T. C. Image guidance doses delivered during radiotherapy: Quantification, management, and reduction: Report of the AAPM Therapy Physics Committee Task Group 180. **Medical Physics**, Alexandria, VA: American Association of Physicists in Medicine, v. 45, n. 5, p. e1121–e1146, 2018

[2] BISSONNETTE, J.-P.; BALTER, P. A.; DONG, L.; LANGEN, K. M.; LOVEOCK, D. M.; MIFTEN, M.; MOSELEY, D. J.; POULIOT, J.; SONKE, J.-J.; YOO, S. Quality assurance for image-guided radiation therapy utilizing CT-based technologies: A report of the AAPM TG-179. **Medical Physics**, Alexandria, VA: American Association of Physicists in Medicine, v. 39, n. 4, p. 1741–1763, 2012. DOI: 10.1118/1.3690466

[3] OLIVEIRA, J.B.; NERSISSIAN, D.Y.; YOSHIMURA, E.M. Tomografia computadorizada de feixe cônico (CBCT) em radioterapia guiada por imagem (IGRT): dosimetria e qualidade de imagem [Internet]. São Paulo: Faculdade de Medicina da Universidade de São Paulo; 2021 [cited 2025 Nov 7]. Trabalho de conclusão de curso (Residência em Medicina).

[4] KERNS, J.R. Pylinac: Image analysis for routine quality assurance in radiotherapy [Internet]. Version 3.39.0. 2023 [cited 2025 Nov 07]. Available from: https://pylinac.readthedocs.io/en/latest/

[5] The Phantom Laboratory, Inc. Catphan® 503 Manual. Greenwich, NY: The Phantom Laboratory, Inc.; 2017

[6] DOWNES, P.; JARVIS, R.; RADU, E.; KAWRAKOW, I.; SPEZI, E. Monte Carlo simulation and patient dosimetry for a kilovoltage cone-beam CT unit. **Medical Physics**. 2009 Sep;36(9):4156-4167. doi:10.1118/1.3196182.

[7] AL-KABKABI, A.; RAMACHANDRAN, P.; AAMRY, A.; TAMAM, N.; ABUHADI, N. H.; JOHARY, Y.; AAMRI, H.; SULIEMAN, A.; TRAPP, J. Assessment of cone beam computed tomography image quality and dose for commonly used pre-sets in external beam radiotherapy. **Radiation Physics and Chemistry**. 2022; 199:110287. doi:10.1016/j.radphyschem.2022.110287.

[8] WILSON, L. J.; HADJIPANTELI, A.; ØSTERGAARD, D. E.; BOGAERT, E.; BROWN, K. F.; DEJONG, R.; EARLEY, J.; EDOUARD, M.; KHAN, M.; LINDSAY, J.; VAN DER HIMST, J.; DING, G. X.; WOOD, T.; AZNAR, M. C.; JORNET, N.; NTENTAS, G. ET AL. (2025). Cone Beam CT Dose Optimisation: A Review and Expert Consensus by the 2022 ESTRO Physics Workshop IGRT Working Group. **Radiotherapy and Oncology**, 209, Article 110958. https://doi.org/10.1016/j.radonc.2025.110958

[9] KAMATH S.; SONG W.; CHVETSOV A.; OZAWA S.; LU H.; SAMANT S.; LIU C.; LI J.G.; PALTA J.R. An image quality comparison study between XVI and OBI CBCT systems. **Journal of Applied Clinical Medical Physics**. 2011 Feb 4;12(2):376-390. DOI: 10.1120/jacmp.v12i2.3435.

LICENSE